

The square-kagome quantum Heisenberg antiferromagnet at high magnetic fields: The localized-magnon paradigm and beyond

Oleg Derzhko

*Institute for Condensed Matter Physics,
National Academy of Sciences of Ukraine,
1 Svientsitskii Street, L'viv-11, 79011, Ukraine*

*Department for Theoretical Physics,
Ivan Franko National University of L'viv,
12 Drahomanov Street, L'viv-5, 79005, Ukraine and
Abdus Salam International Centre for Theoretical Physics,
Strada Costiera 11, I-34151 Trieste, Italy*

Johannes Richter

*Institut für theoretische Physik, Otto-von-Guericke-Universität Magdeburg,
P.O. Box 4120, D-39016 Magdeburg, Germany*

Olesia Krupnitska

*Institute for Condensed Matter Physics,
National Academy of Sciences of Ukraine,
1 Svientsitskii Street, L'viv-11, 79011, Ukraine*

Taras Krokhmalskii

*Institute for Condensed Matter Physics,
National Academy of Sciences of Ukraine,
1 Svientsitskii Street, L'viv-11, 79011, Ukraine and
Department for Theoretical Physics,
Ivan Franko National University of L'viv,
12 Drahomanov Street, L'viv-5, 79005, Ukraine*

(Dated: June 9, 2018)

Abstract

We consider the spin-1/2 antiferromagnetic Heisenberg model on the two-dimensional square-kagome lattice with almost dispersionless lowest magnon band. For a general exchange coupling geometry we elaborate low-energy effective Hamiltonians which emerge at high magnetic fields. The effective model to describe the low-energy degrees of freedom of the initial frustrated quantum spin model is the (unfrustrated) square-lattice spin-1/2 XXZ model in a z -aligned magnetic field. For the effective model we perform quantum Monte Carlo simulations to discuss the low-temperature properties of the square-kagome quantum Heisenberg antiferromagnet at high magnetic fields. We pay special attention to a magnetic-field driven Berezinskii-Kosterlitz-Thouless phase transition which occurs at low temperatures.

PACS numbers: 75.10.Jm

Keywords: quantum Heisenberg antiferromagnet, square-kagome lattice, localized magnons, Berezinskii-Kosterlitz-Thouless transition

I. INTRODUCTION

Antiferromagnetic interactions between the spins carried by magnetic ions placed on a nonbipartite lattice (like the triangle lattice or the kagome lattice) are competing, i.e., frustrated. The Zeeman interaction with an external magnetic field introduces even more competition. As a result, the quantum Heisenberg antiferromagnet on a low-dimensional nonbipartite lattice in a magnetic field provides an excellent playground for the study of the interplay between quantum fluctuations and frustration. In such systems new phenomena may emerge. Therefore, the study of frustrated quantum antiferromagnets attracts much attention nowadays.[1] Interestingly, in some cases frustrated quantum Heisenberg antiferromagnets admit a rather detailed study of their low-temperature properties at high magnetic fields, namely for the so-called localized-magnon systems which have a dispersionless (flat) lowest magnon band.[2, 3] It has been shown that the localized-magnon systems in the high-field low-temperature regime may be understood using specific methods of classical statistical mechanics.[2–8] However, this classical description of the localized-magnon quantum spin systems was developed under the assumption of the so-called ideal geometry, i.e., the conditions for localization of the magnon states are strictly fulfilled (i.e., the lowest magnon band is strictly flat). As a rule, this assumption is violated in real-life systems. Hence, the case of nonideal geometry, when the localization condition is (slightly) violated, is more relevant from the experimental point of view. There were several papers related to this nonideal situation,[9–13] which, however, did not use the localized-magnon paradigm.

Recently[14] we have developed a systematic treatment of a certain class of localized-magnon systems, namely the monomer class,[6] to consider small deviations from ideal geometry. In particular, we have investigated the antiferromagnetic quantum Heisenberg model in a field on the diamond chain, the dimer-plaquette chain, and the square-kagome lattice (for the latter lattice see Fig. 1). We mention that all of these models of frustrated quantum antiferromagnets have attracted attention previously as strongly frustrated quantum spin systems, and they were investigated by various authors also at zero or moderate fields, where the localized-magnon scenario is not relevant, see Refs. 15–17. Inspired by the situation in the diamond-chain like compound azurite,[12, 18, 19] in Ref. 14 it was assumed that $J_{25} = J_{54} = J_{36} = J_{61} = J_1$ and $J_{15} = J_{53} = J_{26} = J_{64} = J_3$ (cf. Fig. 1) that we will call azurite-like geometry. For that type of exchange geometry, by eliminating high-energy de-

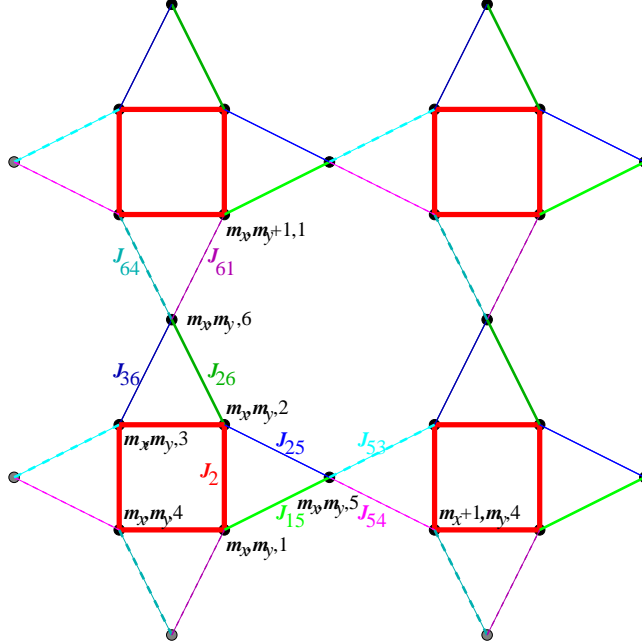


FIG. 1: (Color online) The square-kagome lattice described by Hamiltonian (2.1). The trapping cells for localized magnons (squares) are indicated by bold red lines (J_2 bonds).

degrees of freedom, we constructed several low-energy effective Hamiltonians which are much simpler to treat than the initial ones. Thus for the N -site frustrated square-kagome lattice with the azurite-like deviation from ideal geometry[12, 19] we obtained the Hamiltonian of the \mathcal{N} -site ($\mathcal{N} = N/6$) unfrustrated square-lattice (pseudo)spin-1/2 XXZ model in a z -aligned magnetic field. Then we performed exact-diagonalization studies for the obtained effective model of $\mathcal{N} = 20$ sites (corresponding to $N = 120$ sites for the initial square-kagome system) to discuss the low-temperature properties of the spin-1/2 square-kagome Heisenberg antiferromagnet in a field. The most intriguing feature that we found in Ref. 14 is the existence of a magnetic-field driven Berezinskii-Kosterlitz-Thouless (BKT) phase transition at low temperatures.

The aim of the present paper, which continues the preceding study[14] with a special focus on the square-kagome system, is three-fold. First, we will provide effective Hamiltonians for a general exchange coupling scheme, see Fig. 1, going beyond the the azurite-like geometry. (Besides, we will report in Appendix A similar results for the one-dimensional diamond-chain case.) Second, instead of the exact-diagonalization method that is restricted to small systems only, we now present data obtained by quantum Monte Carlo simulations

for the effective model of much larger size up to $\mathcal{N} = 24 \times 24 = 576$ sites (corresponding to $N = 3456$ sites for the initial square-kagome system). Based on these data we are able to make more precise predictions for the high-field low-temperature properties of the square-kagome quantum Heisenberg antiferromagnet, in particular, for the phase diagram of the model. Third, we will provide a more detailed discussion of the BKT phase transition which may occur in the square-kagome quantum Heisenberg antiferromagnet emphasizing some tasks for further studies.

II. LOW-ENERGY EFFECTIVE HAMILTONIANS AT HIGH MAGNETIC FIELDS

In this paper, we consider the standard spin-1/2 antiferromagnetic isotropic Heisenberg model in a magnetic field with the Hamiltonian

$$H = \sum_{(ij)} J_{ij} \mathbf{s}_i \cdot \mathbf{s}_j - h S^z, \quad S^z = \sum_{i=1}^N s_i^z, \quad J_{ij} > 0. \quad (2.1)$$

Here the first sum runs over all nearest-neighbor bonds on the square-kagome lattice, whereas the second one runs over all N lattice sites. It is convenient to label the sites by a pair of indices, where the first vector index $\mathbf{m} = (m_x, m_y)$ enumerates the $\mathcal{N} = N/6$ unit cells and the second one enumerates the position of the site within the unit cell, see Fig. 1. Since $[S^z, H] = 0$, the eigenvalues of S^z are good quantum numbers. We consider magnetic fields in the vicinity of the saturation field h_{sat} . For the ideal geometry, when $J_{15} = \dots = J_{64} = J \leq J_2$, we have $h_{\text{sat}} = h_1 = 2J_2 + J$. Then for $h > h_1$ the ground state is the fully polarized ferromagnetic state, and the band of the lowest-magnon excitations is dispersionless (flat). An eigenstate from this band can be written as a localized-magnon state,[2] where the spin-flip (magnon) is trapped on a square (trapping cell), see Fig. 1. Owing to the localized nature of these states the many-magnon states in the subspaces $S^z = N/2 - 2, \dots, N/2 - \mathcal{N}$ can be constructed by filling the traps by localized magnons. Clearly, all these states are linear independent.[20] Moreover, these localized-magnon states have the lowest energy in their corresponding S^z -subspace, if the strength of the antiferromagnetic bonds of the trapping cells J_2 exceeds a lower bound.[2, 21] The degeneracy of the localized-magnon states is calculated via mapping of these states onto spatial configurations of hard monomers on an auxiliary square lattice.[5, 6] At low temperatures and for magnetic fields h around the

saturation field $h_{\text{sat}} = h_1$ the contribution of localized-magnon states dominates the partition function.[6]

In what follows we consider the most general violation of the ideal geometry by allowing that all values of J_{15}, \dots, J_{64} are different, see Fig. 1. However, we assume that the deviations from ideal geometry are not too large, i.e., perturbation theory is applicable. To derive the effective Hamiltonian we follow closely the lines given in Ref. 14.

At high fields considered here, only a few states of the trapping cell are relevant, namely, the fully polarized state $|u\rangle = |\uparrow_1\uparrow_2\uparrow_3\uparrow_4\rangle$ with the energy $J_2 - 2h$ and the one-magnon state $|d\rangle = (|\uparrow_1\uparrow_2\uparrow_3\downarrow_4\rangle - |\uparrow_1\uparrow_2\downarrow_3\uparrow_4\rangle + |\uparrow_1\downarrow_2\uparrow_3\uparrow_4\rangle - |\downarrow_1\uparrow_2\uparrow_3\uparrow_4\rangle)/2$ with the energy $-J_2 - h$. All other sites carry fully polarized (i.e., z -aligned) spins. Decreasing the magnetic field from $h > h_1$ to $h < h_1$, in the case of ideal geometry, the ground state of the cell undergoes a transition from the state $|u\rangle$ to the state $|d\rangle$ at the saturation field $h_{\text{sat}} = h_1$. Therefore it is a reasonable approximation to take into account further only these 2 most relevant states $|u\rangle$ and $|d\rangle$ for each square instead of the complete set of 16 states of a square. According to Ref. 14, we use this restricted set of states and consider as the starting point instead of H (2.1) the projected Hamiltonian

$$\begin{aligned} \mathcal{H} &= \mathcal{P}H\mathcal{P}, \\ \mathcal{P} &= \otimes_{\mathbf{m}} \mathcal{P}_{\mathbf{m}}, \quad \mathcal{P}_{\mathbf{m}} = (|u\rangle\langle u| + |d\rangle\langle d|)_{\mathbf{m}}. \end{aligned} \tag{2.2}$$

Here $\mathcal{P}_{\mathbf{m}}$ is the projector on the relevant states of the trapping cell \mathbf{m} . Introducing (pseudo)spin-1/2 operators for each cell,

$$T^z = \frac{1}{2} (|u\rangle\langle u| - |d\rangle\langle d|), T^+ = |u\rangle\langle d|, T^- = |d\rangle\langle u|, \tag{2.3}$$

we can write the Hamiltonian \mathcal{H} in Eq. (2.2) as

$$\begin{aligned}
\mathcal{H} = \sum_{\mathbf{m}} & \left[-\frac{3}{2}h - (h - 2J_2) T_{\mathbf{m}}^z \right. \\
& - \left(h - \frac{3}{2}J_h \right) s_{\mathbf{m},5}^z - \left(h - \frac{3}{2}J_v \right) s_{\mathbf{m},6}^z \\
& \quad + \frac{J_{15} + J_{25}}{4} T_{\mathbf{m}}^z s_{\mathbf{m},5}^z \\
& \quad + \frac{-J_{15} + J_{25}}{2} (T_{\mathbf{m}}^x s_{\mathbf{m},5}^x + T_{\mathbf{m}}^y s_{\mathbf{m},5}^y) \\
& \quad \quad + \frac{J_{54} + J_{53}}{4} s_{\mathbf{m},5}^z T_{m_x+1, m_y}^z \\
& + \frac{J_{54} - J_{53}}{2} \left(s_{\mathbf{m},5}^x T_{m_x+1, m_y}^x + s_{\mathbf{m},5}^y T_{m_x+1, m_y}^y \right) \\
& \quad \quad + \frac{J_{26} + J_{36}}{4} T_{\mathbf{m}}^z s_{\mathbf{m},6}^z \\
& \quad + \frac{J_{26} - J_{36}}{2} (T_{\mathbf{m}}^x s_{\mathbf{m},6}^x + T_{\mathbf{m}}^y s_{\mathbf{m},6}^y) \\
& \quad \quad + \frac{J_{61} + J_{64}}{4} s_{\mathbf{m},6}^z T_{m_x, m_y+1}^z \\
& \left. + \frac{-J_{61} + J_{64}}{2} \left(s_{\mathbf{m},6}^x T_{m_x, m_y+1}^x + s_{\mathbf{m},6}^y T_{m_x, m_y+1}^y \right) \right], \\
J_h & = \frac{J_{15} + J_{25} + J_{54} + J_{53}}{4}, \\
J_v & = \frac{J_{26} + J_{36} + J_{61} + J_{64}}{4}. \tag{2.4}
\end{aligned}$$

This Hamiltonian \mathcal{H} corresponds to a spin-1/2 XXZ model on a decorated square lattice (which is also known as the Lieb lattice[22]).

Although the obtained effective model (2.4) is unfrustrated and therefore is much easier to study (for example, using quantum Monte Carlo simulations), it can be further simplified by eliminating the spin variables $\mathbf{s}_{\mathbf{m},5}$ and $\mathbf{s}_{\mathbf{m},6}$ belonging to the sites which connect the squares by treating small deviations from the ideal geometry perturbatively. More specifically, the Hamiltonian \mathcal{H} given in Eq. (2.4) is separated into a ‘‘main’’ part $\mathcal{H}_{\text{main}}$

$$\begin{aligned}
\mathcal{H}_{\text{main}} = \sum_{\mathbf{m}} & \left[-\frac{3}{2}h_1 - (h_1 - 2J_2) T_{\mathbf{m}}^z \right. \\
& - \left(h_1 - \frac{3}{2}J \right) (s_{\mathbf{m},5}^z + s_{\mathbf{m},6}^z) \\
& + \frac{J}{2} \left(T_{\mathbf{m}}^z s_{\mathbf{m},5}^z + s_{\mathbf{m},5}^z T_{m_x+1, m_y}^z \right. \\
& \quad \left. + T_{\mathbf{m}}^z s_{\mathbf{m},6}^z + s_{\mathbf{m},6}^z T_{m_x, m_y+1}^z \right) \left. \right] \tag{2.5}
\end{aligned}$$

[i.e., the Hamiltonian \mathcal{H} for the ideal geometry case $J_{15} = \dots = J_{64} = J = (J_{15} + \dots + J_{64})/8$ at $h = h_1 = 2J_2 + J$] and a ‘‘perturbation’’ \mathcal{V}

$$\begin{aligned}
\mathcal{V} = \sum_{\mathbf{m}} \left\{ & -\frac{3}{2} (h - h_1) - (h - h_1) T_{\mathbf{m}}^z \right. \\
& - \left[h - h_1 - \frac{3}{2} (J_h - J) \right] s_{\mathbf{m},5}^z \\
& - \left[h - h_1 - \frac{3}{2} (J_v - J) \right] s_{\mathbf{m},6}^z \\
& + \frac{J_{15} + J_{25} - 2J}{4} T_{\mathbf{m}}^z s_{\mathbf{m},5}^z \\
& + \frac{-J_{15} + J_{25}}{2} (T_{\mathbf{m}}^x s_{\mathbf{m},5}^x + T_{\mathbf{m}}^y s_{\mathbf{m},5}^y) \\
& + \frac{J_{54} + J_{53} - 2J}{4} s_{\mathbf{m},5}^z T_{m_x+1, m_y}^z \\
& + \frac{J_{54} - J_{53}}{2} \left(s_{\mathbf{m},5}^x T_{m_x+1, m_y}^x + s_{\mathbf{m},5}^y T_{m_x+1, m_y}^y \right) \\
& + \frac{J_{26} + J_{36} - 2J}{4} T_{\mathbf{m}}^z s_{\mathbf{m},6}^z \\
& + \frac{J_{26} - J_{36}}{2} (T_{\mathbf{m}}^x s_{\mathbf{m},6}^x + T_{\mathbf{m}}^y s_{\mathbf{m},6}^y) \\
& + \frac{J_{61} + J_{64} - 2J}{4} s_{\mathbf{m},6}^z T_{m_x, m_y+1}^z \\
& \left. + \frac{-J_{61} + J_{64}}{2} \left(s_{\mathbf{m},6}^x T_{m_x, m_y+1}^x + s_{\mathbf{m},6}^y T_{m_x, m_y+1}^y \right) \right\} \quad (2.6)
\end{aligned}$$

(i.e., $\mathcal{V} = \mathcal{H} - \mathcal{H}_{\text{main}}$). The ground state $|\varphi_0\rangle$ of the Hamiltonian $\mathcal{H}_{\text{main}}$ (then $s_{\mathbf{m},5}^z = s_{\mathbf{m},6}^z = 1/2$) has the energy $\varepsilon_0 = -(5J_2 + J)\mathcal{N}$. It is $2^{\mathcal{N}}$ -fold degenerate (since it does not depend on the value of $T_{\mathbf{m}}^z = \pm 1/2$) and forms a model space defined by the projector $P = |\varphi_0\rangle\langle\varphi_0|$. Explicitly this projector can be written as

$$\begin{aligned}
P &= \otimes_{\mathbf{m}} P_{\mathbf{m}}, \\
P_{\mathbf{m}} &= \mathcal{P}_{\mathbf{m}} \otimes (|\uparrow_5\rangle\langle\uparrow_5| \otimes |\uparrow_6\rangle\langle\uparrow_6|)_{\mathbf{m}}. \quad (2.7)
\end{aligned}$$

For $J_{15} - J \neq 0, \dots, J_{64} - J \neq 0$, and $h - h_1 \neq 0$ we construct an effective Hamiltonian \mathcal{H}_{eff} which acts on the model space only but which gives the exact ground-state energy. \mathcal{H}_{eff} can be found perturbatively and it is given by[23–25]

$$\mathcal{H}_{\text{eff}} = P\mathcal{H}P + P\mathcal{V} \sum_{\alpha \neq 0} \frac{|\varphi_{\alpha}\rangle\langle\varphi_{\alpha}|}{\varepsilon_0 - \varepsilon_{\alpha}} \mathcal{V}P + \dots \quad (2.8)$$

Here $|\varphi_{\alpha}\rangle$ ($\alpha \neq 0$) are the known excited states of $\mathcal{H}_{\text{main}}$ (2.5). The set of relevant excited states which enters the second term in Eq. (2.8) is constituted of the states with one flipped

spin on those sites that connect two neighboring squares. The energy of the excited states depends on the states of these two squares. Namely, it acquires the value $\varepsilon_\alpha = \varepsilon_0 + 2J_2 - J$ if both squares are in the $|u\rangle$ state, the value $\varepsilon_\alpha = \varepsilon_0 + 2J_2 - J/2$ if one of the squares is in the $|u\rangle$ state and the other one in the $|d\rangle$ state, and the value $\varepsilon_\alpha = \varepsilon_0 + 2J_2$ if both squares are in the $|d\rangle$ state. Taking this into account, we can calculate the second term of Eq. (2.8) and after using (pseudo)spin operators (2.3) we finally arrive at the Hamiltonian

$$\mathcal{H}_{\text{eff}} = \sum_{(mn)} [\mathbf{J}_{mn} (T_m^x T_n^x + T_m^y T_n^y) + J_{mn}^z T_m^z T_n^z] - \mathbf{h} \sum_{m=1}^{\mathcal{N}} T_m^z + \mathcal{N}\mathbf{C}, \quad (2.9)$$

where the first sum runs over the neighboring sites of an \mathcal{N} -site square lattice. The parameters \mathbf{J}_{mn} , J_{mn}^z , \mathbf{h} , and \mathbf{C} are given by

$$\begin{aligned} J_h &= -\frac{(-J_{15} + J_{25})(J_{54} - J_{53})}{16J_2} \frac{1}{1 - \frac{J}{2J_2}}, \\ J_v &= -\frac{(J_{26} - J_{36})(-J_{61} + J_{64})}{16J_2} \frac{1}{1 - \frac{J}{2J_2}}, \\ J_h^z &= \frac{S_h}{16J_2} \left(\frac{1}{1 - \frac{J}{2J_2}} - \frac{1}{1 - \frac{J}{4J_2}} \right), \\ J_v^z &= \frac{S_v}{16J_2} \left(\frac{1}{1 - \frac{J}{2J_2}} - \frac{1}{1 - \frac{J}{4J_2}} \right), \\ \mathbf{h} &= h - h_1 - \frac{S_h + S_v}{16J_2} \frac{1}{1 - \frac{J}{4J_2}}, \\ \mathbf{C} &= -\frac{5}{2}h + \frac{3}{2}J \\ &\quad - \frac{S_h + S_v}{64J_2} \left(\frac{1}{1 - \frac{J}{2J_2}} + \frac{1}{1 - \frac{J}{4J_2}} \right), \\ J &= \frac{J_{15} + J_{25} + J_{54} + J_{53} + J_{26} + J_{36} + J_{61} + J_{64}}{8}, \\ S_h &= \frac{(-J_{15} + J_{25})^2 + (J_{54} - J_{53})^2}{2}, \\ S_v &= \frac{(J_{26} - J_{36})^2 + (-J_{61} + J_{64})^2}{2}, \\ h_1 &= 2J_2 + J. \end{aligned} \quad (2.10)$$

Here the index h (v) corresponds to the horizontal (vertical) direction. For the special case $J_{25} = J_{54} = J_{36} = J_{61} = J_1$ and $J_{15} = J_{53} = J_{26} = J_{64} = J_3$ Eqs. (2.9) and (2.10) transform

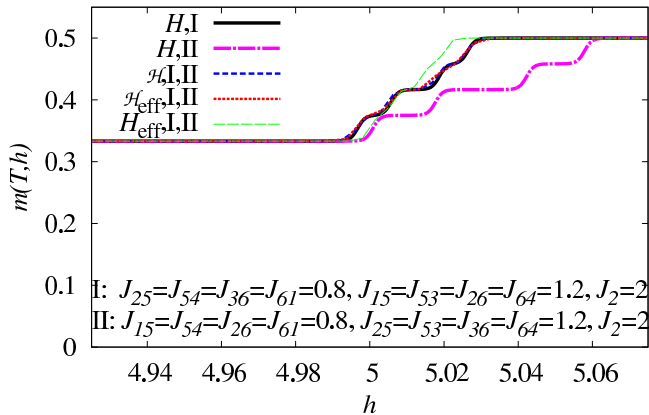


FIG. 2: (Color online) Field dependence of the low-temperature magnetization per site m of the full and effective models for the distorted square-kagome lattice of $\mathcal{N} = 4$ cells ($T = 0.001$). The first set of parameters (I) corresponds to the azurite-like nonideal geometry: $J_{25} = J_{54} = J_{36} = J_{61} = 0.8$, $J_{15} = J_{53} = J_{26} = J_{64} = 1.2$, $J_2 = 2$ [cf. Fig. 5(a) of Ref. 14]. The second set of parameters (II) is as follows: $J_{15} = J_{54} = J_{26} = J_{61} = 0.8$, $J_{25} = J_{53} = J_{36} = J_{64} = 1.2$, $J_2 = 2$.

into Eqs. (3.10) and (3.11) of Ref. 14.

In the limit $J/J_2 \rightarrow 0$ Eqs. (2.9) and (2.10) transform into the effective Hamiltonian H_{eff} obtained by the strong-coupling approximation with the parameters

$$\begin{aligned}
 J_h &= -\frac{(-J_{15} + J_{25})(J_{54} - J_{53})}{16J_2}, \\
 J_v &= -\frac{(J_{26} - J_{36})(-J_{61} + J_{64})}{16J_2}, \\
 J_h^z &= J_v^z = 0, \\
 \mathbf{h} &= h - h_1 - \frac{S_h + S_v}{16J_2}, \\
 \mathbf{C} &= -\frac{5}{2}h + \frac{3}{2}J - \frac{S_h + S_v}{32J_2}.
 \end{aligned} \tag{2.11}$$

In this limit the effective Hamiltonian is the square-lattice spin-1/2 isotropic XY model in a transverse magnetic field. Again Eq. (2.11) transforms into Eq. (A7) of Ref. 14 for the azurite-like nonideal geometry.

The considered case of a general nonideal geometry allows us to discuss the quality of the elaborated effective description. The effective theories are based on accounting of only two states for each square, $|u\rangle$ and $|d\rangle$, and may overestimate a tendency for localization. This can be seen already from inspection of the constants J_h and J_v given in Eqs. (2.10) and (2.11).

According to these formulas, having, for example, $J_{15} = J_{25}$ and $J_{26} = J_{36}$ but $J_{53} \neq J_{54}$ and $J_{61} \neq J_{64}$ would be sufficient to suppress completely a spreading of localized states over the lattice. By contrast, exact-diagonalization results (not shown here) demonstrate that this condition is not sufficient to avoid the spreading, rather we need in addition the equalities $J_{53} = J_{54}$ and $J_{61} = J_{64}$. In Fig. 2 we compare exact-diagonalization data for the low-temperature magnetization curve calculated for the full model of $N = 24$ sites for two sets of parameters, $J_{25} = J_{54} = J_{36} = J_{61} = 0.8$, $J_{15} = J_{53} = J_{26} = J_{64} = 1.2$, $J_2 = 2$ [the azurite-like nonideal geometry, cf. Fig. 5(a) of Ref. 14] and $J_{15} = J_{54} = J_{26} = J_{61} = 0.8$, $J_{25} = J_{53} = J_{36} = J_{64} = 1.2$, $J_2 = 2$, with the predictions obtained from corresponding effective models (2.4), (2.9), (2.10), and (2.9), (2.11). For this choice both sets yield identical results within each of the effective theories, but both sets lead to different results for the full initial model. While for the first set the effective models (except the strong coupling-approximation) work well, see the short-dashed blue curves and dotted red curves in Fig. 2, for the second data set the agreement is less satisfactory, since the initial model exhibits a wider field region where magnetization varies between the two plateau values, $m = 1/3$ and $m = 1/2$ (dash-dotted magenta curve in Fig. 2). In the latter case a discrepancy emerges already between the results which follow from H (2.1) and \mathcal{H} (2.2), which leads to the conclusion that the restriction to only two states of each square yields excellent or only modest results depending on specific nonideal geometry under consideration.

Similar to model (2.4), the obtained spin lattice models (2.9), (2.10) and (2.9), (2.11) are also unfrustrated, however, they are simpler and have less sites $\mathcal{N} = N/6$. Therefore they are more appropriate for further analysis using, for example, quantum Monte Carlo techniques. We will report such quantum Monte Carlo results in the next section.

III. HIGH-FIELD LOW-TEMPERATURE SPECIFIC HEAT AND PHASE DIAGRAM

After having derived the effective models (2.9), (2.10) and (2.9), (2.11), the beautiful results known for the square-lattice spin-1/2 XX_0/XXZ Heisenberg model in a z -aligned magnetic field can be used to understand the high-field low-temperature properties of the square-kagome quantum Heisenberg antiferromagnet. Since we know that our effective models work very well for azurite-like distortions of ideal geometry (see the above discussion),

in what follows we restrict ourselves to this case and consider the specific parameter set $J_1 = 0.8$, $J_2 = 2$, and $J_3 = 1.2$. For this set of parameters exact-diagonalization data have been reported already in Ref. 14. However, those results were restricted to small systems up to $\mathcal{N} = 20$. Now we again consider the effective model \mathcal{H}_{eff} given in Eqs. (2.9) and (2.10) but present results of more time-demanding quantum Monte Carlo calculations which refer to much larger systems up to $\mathcal{N} = 24 \times 24 = 576$. To perform these calculations we used the `dirloop_sse` package (the directed loop algorithm in the stochastic series expansion representation) from the ALPS library.[26] For concreteness we will focus on the temperature dependence of the specific heat per site $c(T, h)$ which may be quite sensible to the system size \mathcal{N} (in contrast, for example, to the temperature dependence of the magnetization which shows no size effect). It should be noted that the effective spin models were investigated via quantum Monte Carlo simulations in the past for particular parameter sets. Note further that these models are also considered in the context of hard-core bosons, where the z -aligned magnetization corresponds to the particle number and the magnetic field to the chemical potential.[27] Although these previous studies[28–37] provide a physical picture in general, we have here to perform specific calculations for the effective model with special parameter sets corresponding to the distorted square-kagome quantum Heisenberg antiferromagnet at hand.

From preceding studies (see Ref. 14) we know that deviations from the ideal geometry lead to the following modifications in a small region of h around the saturation field $h_{\text{sat}} = h_1$. (i) Instead of the jump of the ground-state magnetization $m(T = 0)$ at h_1 from a plateau at $m = 1/3$ to saturated magnetization $m = 1/2$, there is a small finite region $h_{1l} \leq h \leq h_{1h}$ around h_1 (for $J_1 = 0.8$, $J_2 = 2$, and $J_3 = 1.2$ we have $h_1 = 5$, $h_{1l} \approx 4.996$, $h_{1h} \approx 5.027$) where the magnetization shows a steep increase between the two plateau values, $m = 1/3$ and $m = 1/2$. (ii) Instead of a nonzero residual entropy at h_1 , there is zero residual entropy followed by a strong enhancement of the entropy at very small temperatures. (iii) Instead of zero specific heat at h_1 , the specific heat $c(T)$ shows a T^2 -decay as $T \rightarrow 0$ in a small region of h around h_1 , but it vanishes exponentially as $T \rightarrow 0$ in the plateau regions, i.e., in the gapped phase. Our quantum Monte Carlo results ($\mathcal{N} = 100, 256, 400, 576$) for the specific heat collected in Fig. 3 support this scenario for the low-temperature behavior of $c(T, h)$. In particular, from Fig. 3 one can find indications for different decay laws as $T \rightarrow 0$ for $h = 4.99$ and $h = 5.03$ (exponential) and for $h = 5.01$ and $h = 5.02$ (power-law). Note,

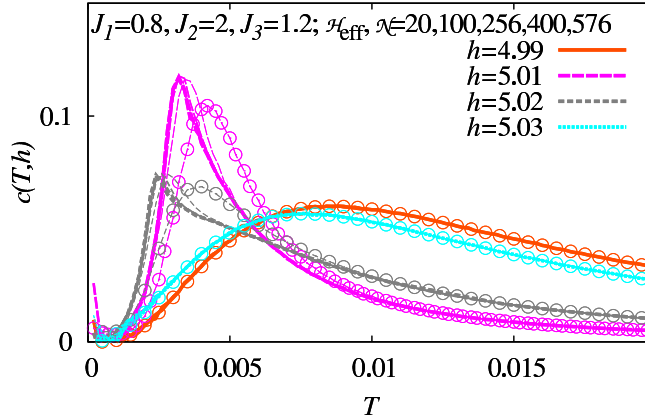


FIG. 3: (Color online) Specific heat per site $c(T, h)$ at high fields ($h = 4.99, 5.01, 5.02, 5.03$) and low temperatures for the distorted square-kagome Heisenberg antiferromagnet (2.1) with $J_1 = 0.8$, $J_2 = 2$, $J_3 = 1.2$ obtained by quantum Monte Carlo simulations for the effective Hamiltonian \mathcal{H}_{eff} (2.9), (2.10) with $\mathcal{N} = 100, 256, 400, 576$ (the line thickness increases with increase of \mathcal{N}). For comparison, we also show exact-diagonalization data for $\mathcal{N} = 20$ by very thin curves with circles [cf. Fig. 11(b) of Ref. 14].

however, that at extremely low temperatures quantum Monte Carlo data become noisy that restricts our consideration to temperatures above $T = 0.0005$. (We note that exact-diagonalization data at extremely low temperatures become also unreliable, since they suffer from finite-size artifacts.) New features with respect to our previous exact-diagonalization study[14] appearing for larger systems are obvious from Fig. 3, where for comparison also exact-diagonalization data for $\mathcal{N} = 20$ are shown. As \mathcal{N} increases, the peak for $h = 5.01$ and $h = 5.02$ becomes somewhat higher and sharper and moves to slightly lower temperatures. For $h = 5.02$ it changes even its form. On the other hand, the temperature profiles for $h = 4.99$ and $h = 5.03$ are insensitive to the system sizes. This behavior of temperature profiles as h varies reflects the difference in the low-temperature specific heat for the gapless phase (h is inside the region $h_{1l} \leq h \leq h_{1h}$) and the gapped phases (h is outside this region).

The most intriguing property of the effective models (2.9), (2.11) and (2.9), (2.10) is the existence of a BKT transition. A classical two-dimensional isotropic XY model undergoes a transition from bound vortex-antivortex pairs at low temperatures to unpaired vortices and antivortices at some critical temperature T_c . [38] For $T < T_c$ (superfluid phase) the system is characterized by quasi-long-range order, i.e., correlations decay algebraically at

large distances without the emergence of a nonvanishing order parameter. For $T > T_c$ (normal phase) the system is disordered with an exponential increase of the correlation length ξ as $T \rightarrow T_c$,

$$\xi \propto e^{\frac{b}{\sqrt{\tau}}}, \quad \tau = \frac{T - T_c}{T_c}. \quad (3.1)$$

The BKT transition temperature for the classical square-lattice isotropic XY model (without field) is $T_c \approx 0.893|J|$. [39–42] Within numerical studies dealing with finite systems it is quite difficult to extract an exponential divergence of ξ at T_c from the finite-size data for the large-distance behavior of spin correlations. Another important quantity to pin down the BKT transition is the so-called helicity modulus Υ which is related to the superfluid density ρ_s . [43] In the quantum spin-1/2 case, the BKT critical behavior occurs too. [28, 29, 31] The critical temperature for the $s = 1/2$ case is estimated as $T_c \approx 0.34|J|$. [31, 36, 37] The quantum model is gapless with an excitation spectrum that is linear in the momentum. The specific heat $c(T)$ shows T^2 behavior for $T \rightarrow 0$, it increases very rapidly around T_c , and it exhibits a finite peak somewhat above T_c . [29] This kind of the low-temperature thermodynamics survives for not too large z -aligned magnetic field $|h| < 2|J|$ (see, e.g., Figs. 3 and 8 in Ref. 34 or Fig. 1 in Refs. 36 and 37). Also for the spin-1/2 square-lattice XXZ model with dominating isotropic XY interaction in a z -aligned magnetic field the BKT transition appears. [35]

Following our previous study, [14] we use the observation of Ref. 29 that the BKT transition point T_c is located somewhat below the well-pronounced peak-like maximum of the specific heat. Although the adopted criterion to fix the critical temperature T_c for different h is a rather rough one, it can provide a sketch of the phase diagram based on specific-heat data. Since the peak in $c(T)$ calculated by exact diagonalization shows noticeable finite-size effects, [14] we use here the quantum Monte Carlo approach to obtain data for much larger systems thus getting more accurate predictions. A sketch of the phase diagram of the distorted square-kagome Heisenberg antiferromagnet in the $h - T$ plane which uses the maximum in the specific heat as an indicator of the BKT transition is reported in Fig. 4(a). In this figure the thick solid blue line corresponds to the position T^* of the maximum in the specific heat per site $c(T, h)$ obtained by exact diagonalization earlier for $\mathcal{N} = 20$ (cf. Fig. 12 of Ref. 14). The blue symbols correspond to quantum Monte Carlo data ($\mathcal{N} = 100, 256, 400, 576$) for $T^*(h)$. Based on these data for T^* we have drawn the

thick dashed green line showing a tentative BKT-transition line $T_c(h)$. Fig. 4(b) shows the height of the maximum in the specific heat, i.e., the value of $c(T^*, h)$ (here multiplied by 0.12 to get correspondence to Fig. 12 of Ref. 14). Again we compare exact-diagonalization data for $\mathcal{N} = 20$ (thin red line) with new quantum Monte Carlo data for $\mathcal{N} = 100, 256, 400,$ and 576 (symbols). It is obvious that the height of the maximum increases noticeably in the field region where a BKT transition appears. Finally, we illustrate the finite-size dependence of $T^*(h)$ in Fig. 4(c), which is obviously weak. Although $T^*(h)$, $h_{1l} \leq h \leq h_{1h}$, is shifted to slightly lower temperatures for large values \mathcal{N} in comparison with the previous prediction,[14] the values of $T^*(h)$ apparently are already close to their values in the limit $\mathcal{N} \rightarrow \infty$.

IV. CONCLUSIONS

In the present paper we have improved the low-energy theory of the almost flat-band square-kagome quantum Heisenberg antiferromagnet at high magnetic fields. Analytical results for effective Hamiltonians refer now to (small) deviations of general case from the flat-band situation. The relevant effective model has been investigated for quite large system sizes using quantum Monte Carlo simulations. The high-field low-temperature phase diagram of the distorted square-kagome quantum Heisenberg antiferromagnet reported in Fig. 4(a) refines previous findings which were based on exact-diagonalization data for small systems. Although the existence of the BKT transition is not questionable, the precise phase diagram remains an open question. To find precise values for the BKT-transition temperature for the square-kagome quantum Heisenberg antiferromagnet, in fact, one has to determine accurately, e.g., by quantum Monte Carlo techniques, the BKT-transition temperature of the corresponding effective square-lattice spin-1/2 XXZ easy-plane model in a z -aligned magnetic field. To the best of our knowledge, this problem has not been studied yet and its consideration is out of the scope of this article. Finally, the reported results shed more light on possible manifestation of localized-magnon effects in experiments, if a realization of the square-kagome Heisenberg antiferromagnet becomes available.

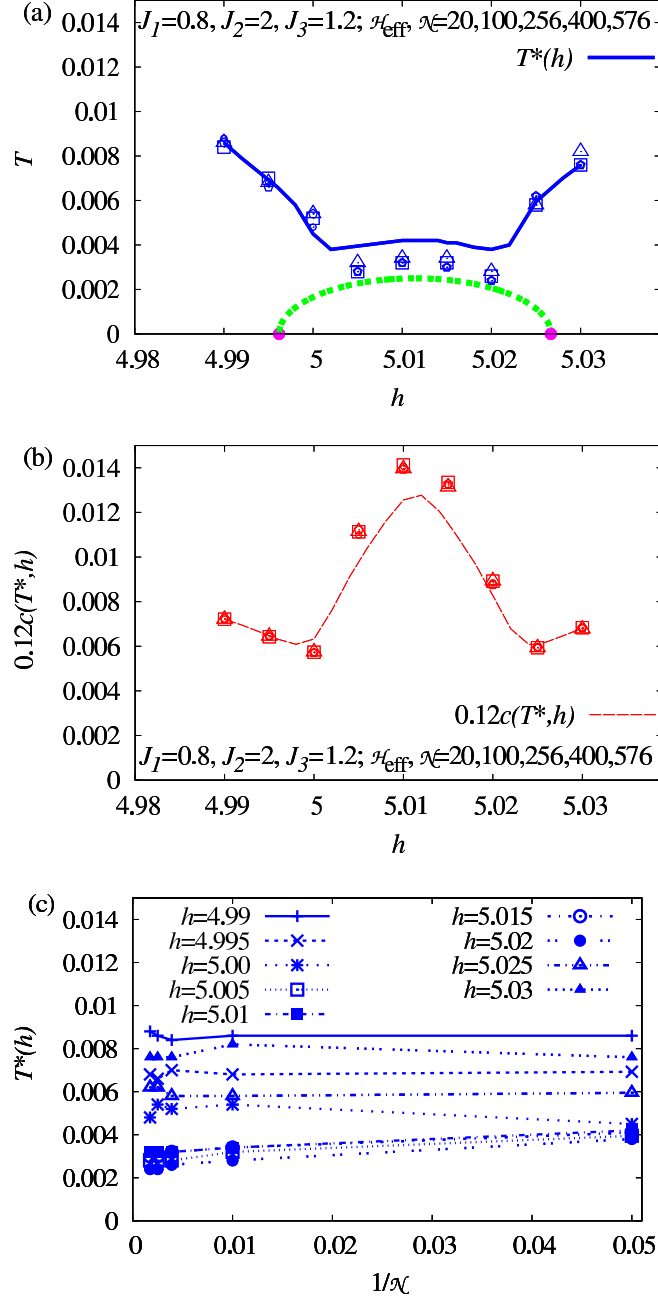


FIG. 4: (Color online) (a) Sketch of the phase diagram of the distorted square-kagome Heisenberg antiferromagnet ($J_1 = 0.8$, $J_2 = 2$, $J_3 = 1.2$) at high magnetic field (thick dashed green line) as it is indicated by the position of the maximum T^* of the specific heat $c(T, h)$ shown by the thick solid blue curve ($\mathcal{N} = 20$) and the blue symbols (triangles – $\mathcal{N} = 100$, squares – $\mathcal{N} = 256$, pentagons – $\mathcal{N} = 400$, circles – $\mathcal{N} = 576$). By filled violet circles the values of $h_{1l} \approx 4.996$ and $h_{1h} \approx 5.027$ are indicated. (b) Height of the maximum in the specific heat $c(T^*, h)$ (multiplied by 0.12): dashed red curve – $\mathcal{N} = 20$, red triangles – $\mathcal{N} = 100$, squares – $\mathcal{N} = 256$, pentagons – $\mathcal{N} = 400$, circles – $\mathcal{N} = 576$. (c) Dependence of $T^*(h)$ on $1/\mathcal{N}$ at various fields h .

Acknowledgments

The present study was supported by the DFG (project RI615/21-1). O. D. acknowledges the kind hospitality of the University of Magdeburg in October-December of 2012 and in March-May of 2013. O. D. acknowledges financial support of the organizers of the 15th CSMAG conference (Košice, 17-21 June 2013) and of the Pavol Jozef Šafárik University in Košice, and of the Abdus Salam International Centre for Theoretical Physics (Trieste, August, 2013). O. D. and J. R. are grateful to the MPIPKS (Dresden) for the kind hospitality in October-December of 2013.

Appendix A: Effective Hamiltonians for the quantum Heisenberg antiferromagnet on a distorted frustrated diamond chain at high magnetic fields

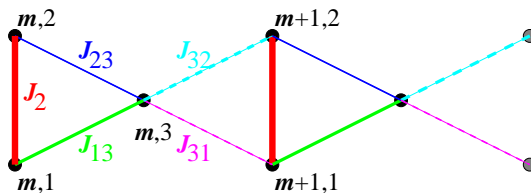


FIG. 5: (Color online) The diamond chain described by Hamiltonian (2.1). The trapping cells for localized magnons (vertical dimers) are indicated by bold red lines (J_2 bonds).

In this appendix we provide a similar extension for the one-dimensional counterpart of the square-kagome lattice, namely the distorted diamond chain, for completeness and comparison. In the case of the diamond chain[15] with a most general exchange coupling scheme [see Eq. (2.1) and Fig. 5] we arrive at the following results. The effective Hamiltonian

\mathcal{H} [cf. Eq. (2.4)] reads

$$\begin{aligned}
\mathcal{H} = \sum_{m=1}^{\mathcal{N}} & \left[-\frac{h}{2} - \frac{J_2}{4} - (h - J_2) T_m^z - (h - J) s_{m,3}^z \right. \\
& + \frac{J_{13} + J_{23}}{2} T_m^z s_{m,3}^z \\
& + \frac{-J_{13} + J_{23}}{\sqrt{2}} (T_m^x s_{m,3}^x + T_m^y s_{m,3}^y) \\
& + \frac{J_{31} + J_{32}}{2} s_{m,3}^z T_{m+1}^z \\
& \left. - \frac{J_{31} - J_{32}}{\sqrt{2}} (s_{m,3}^x T_{m+1}^x + s_{m,3}^y T_{m+1}^y) \right], \\
J = & \frac{J_{13} + J_{23} + J_{31} + J_{32}}{4}.
\end{aligned} \tag{A.1}$$

The effective Hamiltonian \mathcal{H}_{eff} [cf. Eqs. (2.9), (2.10)] is given by the formula

$$\begin{aligned}
\mathcal{H}_{\text{eff}} = \sum_{m=1}^{\mathcal{N}} & \left[J (T_m^x T_{m+1}^x + T_m^y T_{m+1}^y) + J^z T_m^z T_{m+1}^z \right. \\
& \left. - \mathfrak{h} T_m^z + \mathbf{C} \right]
\end{aligned} \tag{A.2}$$

with the following parameters

$$\begin{aligned}
J &= \frac{(-J_{13} + J_{23})(J_{31} - J_{32})}{4J_2} \frac{1}{1 - \frac{J}{J_2}}, \\
J^z &= \frac{(-J_{13} + J_{23})^2 + (J_{31} - J_{32})^2}{8J_2} \left(\frac{1}{1 - \frac{J}{J_2}} - 1 \right), \\
\mathfrak{h} &= h - h_1 - \frac{(-J_{13} + J_{23})^2 + (J_{31} - J_{32})^2}{8J_2}, \\
\mathbf{C} &= -h - \frac{J_2}{4} + \frac{J}{2} \\
& - \frac{(-J_{13} + J_{23})^2 + (J_{31} - J_{32})^2}{32J_2} \left(\frac{1}{1 - \frac{J}{J_2}} + 1 \right), \\
J &= \frac{J_{13} + J_{23} + J_{31} + J_{32}}{4}, \\
h_1 &= J_2 + J.
\end{aligned} \tag{A.3}$$

In the limit $J_{23} = J_{31} = J_1$ and $J_{13} = J_{32} = J_3$ these results coincide with those ones obtained in Ref. 14, see Eqs. (3.6) and (3.7) of Ref. 14.

Similar to the case of the square-kagome lattice, effective theories overestimate the tendency of localization. For example, $J_{13} = J_{23}$ but $J_{31} \neq J_{32}$ or vice versa is sufficient to

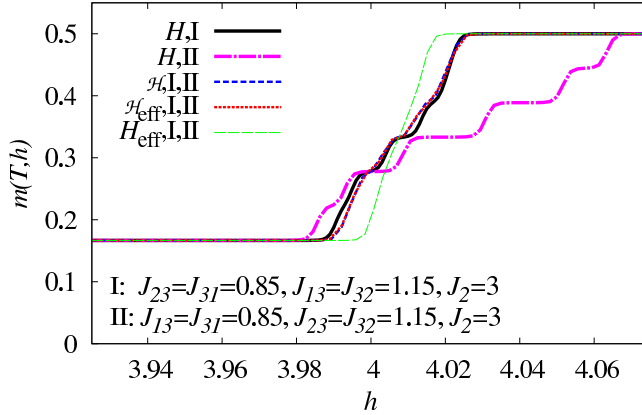


FIG. 6: (Color online) Field dependence of the low-temperature magnetization per site of the full and effective models for the distorted diamond chain of $\mathcal{N} = 6$ cells ($T = 0.001$). The first set of parameters (I) corresponds to the azurite-like nonideal geometry: $J_{23} = J_{31} = 0.85$, $J_{13} = J_{32} = 1.15$, $J_2 = 3$ [cf. Fig. 3(a) of Ref. 14]. The second set of parameters (II) is as follows: $J_{13} = J_{31} = 0.85$, $J_{23} = J_{32} = 1.15$, $J_2 = 3$.

suppress completely a spreading of localized states within the effective models. On the other hand, exact-diagonalization data for the full model indicate that this condition is not sufficient to suppress the spreading, rather we need both equalities to hold, $J_{13} = J_{23}$ but $J_{31} = J_{32}$. In Fig. 6 we compare exact-diagonalization data for the low-temperature magnetization curve for the initial full model and the effective models considering two sets of parameters: $J_{23} = J_{31} = 0.85$, $J_{13} = J_{32} = 1.15$, $J_2 = 3$ [cf. Fig. 3(a) of Ref. 14] and $J_{13} = J_{31} = 0.85$, $J_{23} = J_{32} = 1.15$, $J_2 = 3$. Each effective model yields identical predictions for both sets of parameters, whereas the results for the initial model are different (compare solid black and dash-dotted magenta curves in Fig. 6). Furthermore, for the azurite-like nonideal geometry the effective theory based on Eqs. (A.2), (A.3) provides a quite good quantitative description of the magnetization curve, whereas in the other case the agreement is only qualitative.

[1] C. Lhuillier and G. Misguich, in *High Magnetic Fields: Applications in Condensed Matter Physics and Spectroscopy*, Lecture Notes in Physics Vol. 595, edited by C. Berthier, L. P. Lévy, and G. Martinez (Springer, Berlin, 2002), pp. 161-190; G. Misguich and C. Lhuillier, in *Frus-*

- trated Spin Systems*, edited by H. T. Diep (World Scientific, Singapore, 2005), pp. 229-306; J. Richter, J. Schulenburg, and A. Honecker, in *Quantum Magnetism*, Lecture Notes in Physics Vol. 645, edited by U. Schollwöck, J. Richter, D. J. J. Farnell, and R. F. Bishop (Springer, Berlin, 2004), pp. 85-153.
- [2] J. Schnack, H.-J. Schmidt, J. Richter, and J. Schulenburg, *Eur. Phys. J. B* **24**, 475 (2001); J. Schulenburg, A. Honecker, J. Schnack, J. Richter, and H.-J. Schmidt, *Phys. Rev. Lett.* **88**, 167207 (2002); J. Richter, J. Schulenburg, A. Honecker, J. Schnack, and H.-J. Schmidt, *J. Phys.: Condens. Matter* **16**, S779 (2004).
- [3] J. Richter, O. Derzhko, and J. Schulenburg, *Phys. Rev. Lett.* **93**, 107206 (2004); O. Derzhko and J. Richter, *Phys. Rev. B* **72**, 094437 (2005).
- [4] M. E. Zhitomirsky and H. Tsunetsugu, *Phys. Rev. B* **70**, 100403(R) (2004); M. E. Zhitomirsky and H. Tsunetsugu, *Prog. Theor. Phys. Suppl.* **160**, 361 (2005); M. E. Zhitomirsky and H. Tsunetsugu, *Phys. Rev. B* **75**, 224416 (2007).
- [5] O. Derzhko and J. Richter, *Phys. Rev. B* **70**, 104415 (2004).
- [6] O. Derzhko and J. Richter, *Eur. Phys. J. B* **52**, 23 (2006).
- [7] J. Richter, O. Derzhko, and T. Krokhamalskii, *Phys. Rev. B* **74**, 144430 (2006); O. Derzhko, T. Krokhamalskii, and J. Richter, *Phys. Rev. B* **82**, 214412 (2010).
- [8] M. Maksymenko, O. Derzhko, and J. Richter, *Eur. Phys. J. B* **84**, 397 (2011).
- [9] F. Mila, *Eur. Phys. J. B* **6**, 201 (1998); J.-B. Fouet, F. Mila, D. Clarke, H. Youk, O. Tchernyshyov, P. Fendley, and R. M. Noack, *Phys. Rev. B* **73**, 214405 (2006).
- [10] J.-D. Picon, A. F. Albuquerque, K. P. Schmidt, N. Laflorencie, M. Troyer, and F. Mila, *Phys. Rev. B* **78**, 184418 (2008); A. F. Albuquerque, N. Laflorencie, J.-D. Picon, and F. Mila, *Phys. Rev. B* **83**, 174421 (2011).
- [11] A. Honecker and A. Läuchli, *Phys. Rev. B* **63**, 174407 (2001).
- [12] A. Honecker, S. Hu, R. Peters, and J. Richter, *J. Phys.: Condens. Matter* **23**, 164211 (2011).
- [13] O. Derzhko, J. Richter, and O. Krupnitska, *Condensed Matter Physics (L'viv)* **15**, 43702 (2012).
- [14] O. Derzhko, J. Richter, O. Krupnitska, and T. Krokhamalskii, *Phys. Rev. B* **88**, 094426 (2013).
- [15] K. Takano, K. Kubo, and H. Sakamoto, *J. Phys.: Condens. Matter* **8**, 6405 (1996); H. Niggemann, G. Uimin, and J. Zittartz, *J. Phys.: Condens. Matter* **9**, 9031 (1997); *J. Phys.: Condens. Matter* **10**, 5217 (1998); K. Okamoto, T. Tonegawa, and M. Kaburagi, *J. Phys.: Condens.*

- Matter **15**, 5979 (2003); L. Čanová, J. Strečka, and M. Jaščur, J. Phys.: Condens. Matter **18**, 4967 (2006).
- [16] N. B. Ivanov and J. Richter, Phys. Lett. A **232**, 308 (1997); J. Richter, N. B. Ivanov, and J. Schulenburg, J. Phys.: Condens. Matter **10**, 3635 (1998); A. Koga, K. Okunishi, and N. Kawakami, Phys. Rev. B **62**, 5558 (2000); J. Schulenburg and J. Richter, Phys. Rev. B **65**, 054420 (2002); J. Schulenburg and J. Richter, Phys. Rev. B **66**, 134419 (2002); A. Koga and N. Kawakami, Phys. Rev. B **65**, 214415 (2002); S. R. Manmana, J.-D. Picon, K. P. Schmidt, and F. Mila, Europhys. Lett. **94**, 67004 (2011); V. Ohanyan and A. Honecker, Phys. Rev. B **86**, 054412 (2012); H. G. Paulinelli, S. de Souza, and O. Rojas, J. Phys.: Condens. Matter **25**, 306003 (2013).
- [17] R. Siddharthan and A. Georges, Phys. Rev. B **65**, 014417 (2001); P. Tomczak and J. Richter, J. Phys. A **36**, 5399 (2003); J. Richter, J. Schulenburg, P. Tomczak, and D. Schmalfuß, arXiv:cond-mat/0411673; J. Richter, J. Schulenburg, P. Tomczak, and D. Schmalfuß, Condensed Matter Physics (L'viv) **12**, 507 (2009); H. Nakano and T. Sakai, J. Phys. Soc. Jpn. **82**, 083709 (2013); I. Rousochatzakis, R. Moessner, and J. van den Brink, Phys. Rev. B **88**, 195109 (2013).
- [18] H. Kikuchi, Y. Fujii, M. Chiba, S. Mitsudo, T. Idehara, T. Tonegawa, K. Okamoto, T. Sakai, T. Kuwai, and H. Ohta, Phys. Rev. Lett. **94**, 227201 (2005); H. Kikuchi, Y. Fujii, M. Chiba, S. Mitsudo, T. Idehara, T. Tonegawa, K. Okamoto, T. Sakai, T. Kuwai, K. Kindo, A. Matsuo, W. Higemoto, K. Nishiyama, M. Horvatić, and C. Berthier, Prog. Theor. Phys. Suppl. **159**, 1 (2005).
- [19] H. Jeschke, I. Opahle, H. Kandpal, R. Valenti, H. Das, T. Saha-Dasgupta, O. Janson, H. Rosner, A. Brühl, B. Wolf, M. Lang, J. Richter, S. Hu, X. Wang, R. Peters, T. Pruschke, and A. Honecker, Phys. Rev. Lett. **106**, 217201 (2011).
- [20] H.-J. Schmidt, J. Richter, and R. Moessner, J. Phys. A **39**, 10673 (2006).
- [21] H.-J. Schmidt, J. Phys. A **35**, 6545 (2002).
- [22] E. H. Lieb, Phys. Rev. Lett. **62**, 1201 (1989); **62**, 1927 (1989); H. Tasaki, J. Phys.: Condens. Matter **10**, 4353 (1998).
- [23] D. J. Klein, J. Chem. Phys. **61**, 786 (1974).
- [24] P. Fulde, *Electron Correlations in Molecules and Solids* (Springer-Verlag, Berlin, Heidelberg, 1993), p. 77.

- [25] F. H. L. Essler, H. Frahm, F. Göhmann, A. Klümper, and V. E. Korepin, *The One-Dimensional Hubbard Model* (Cambridge University Press, Cambridge, UK, 2005), p. 38.
- [26] A. F. Albuquerque et. al., *J. Magn. Magn. Mater.* **310**, 1187 (2007); B. Bauer et. al., *J. Stat. Mech.* P05001 (2011).
- [27] The spin-1/2 isotropic XY model can be viewed as the hard-core limit of the Bose-Hubbard model and the z -aligned magnetic field corresponds to the chemical potential. Furthermore, the J^z interaction corresponds to the nearest-neighbor interaction of hard-core bosons. See also T. Matsubara and H. Matsuda, *Prog. Theor. Phys.* **16**, 416 (1956); **16**, 569 (1956); H. Matsuda and T. Matsubara, *Prog. Theor. Phys.* **17**, 19 (1957).
- [28] H.-Q. Ding and M. S. Makivić, *Phys. Rev. B* **42**, 6827 (1990).
- [29] H.-Q. Ding, *Phys. Rev. B* **45**, 230 (1992).
- [30] H.-Q. Ding, *Phys. Rev. Lett.* **68**, 1927 (1992).
- [31] K. Harada and N. Kawashima, *Phys. Rev. B* **55**, R11949 (1997); K. Harada and N. Kawashima, *J. Phys. Soc. Jpn.* **67**, 2768 (1998).
- [32] A. W. Sandvik and C. J. Hamer, *Phys. Rev. B* **60**, 6588 (1999).
- [33] A. Cuccoli, T. Roscilde, V. Tognetti, R. Vaia, and P. Verrucchi, *Phys. Rev. B* **67**, 104414 (2003).
- [34] K. Bernardet, G. G. Batrouni, J.-L. Meunier, G. Schmid, M. Troyer, and A. Dorneich, *Phys. Rev. B* **65**, 104519 (2002).
- [35] F. Hébert, G. G. Batrouni, R. T. Scalettar, G. Schmid, M. Troyer, and A. Dorneich, *Phys. Rev. B* **65**, 014513 (2001); G. Schmid, S. Todo, M. Troyer, and A. Dorneich, *Phys. Rev. Lett.* **88**, 167208 (2002).
- [36] J. Carrasquilla and M. Rigol, *Phys. Rev. A* **86**, 043629 (2012).
- [37] G. Ceccarelli, J. Nespolo, A. Pelissetto, and E. Vicari, *Phys. Rev. B* **88**, 024517 (2013).
- [38] V. L. Berezinskii, *Zh. Eksp. Teor. Fiz.* **59**, 907 (1970) [*Sov. Phys. JETP* **32**, 493 (1971)]; J. M. Kosterlitz and D. J. Thouless, *J. Phys. C* **6**, 1181 (1973); J. M. Kosterlitz, *J. Phys. C* **7**, 1046 (1974); J. V. José, L. P. Kadanoff, S. Kirkpatrick, and D. R. Nelson, *Phys. Rev. B* **16**, 1217 (1977); *Phys. Rev. B* **17**, 1477 (1978).
- [39] R. Gupta, J. DeLapp, G. G. Batrouni, G. C. Fox, C. F. Baillie, and J. Apostolakis, *Phys. Rev. Lett.* **61**, 1996 (1988); R. Gupta and C. F. Baillie, *Phys. Rev. B* **45**, 2883 (1992).
- [40] M. Hasenbusch and K. Pinn, *J. Phys. A* **30**, 63 (1997); M. Hasenbusch, *J. Phys. A* **38**, 5869

(2005).

[41] Y. Komura and Y. Okabe, *J. Phys. Soc. Jpn.* **81**, 113001 (2012).

[42] Y.-D. Hsieh, Y.-J. Kao, and A. W. Sandvik, *J. Stat. Mech.* P09001 (2013).

[43] M. E. Fisher, M. N. Barber, and D. Jasnow, *Phys. Rev. A* **8**, 1111 (1973).